Interferometer Design Proposals for Group Index Extraction in Silicon Photonics

Salvatore Salpietro

***Abstract*—This work presents the design, simulation, fabrication, and experimental testing of integrated interferometric photonic circuits for the extraction of the waveguide group index. Two different Mach–Zehnder interferometer (MZI) architectures are investigated. The first design is based on conventional strip waveguides in both interferometer arms, while the second design includes a grating waveguide in one arm, enabling the analysis of slow-light effects. In both cases, the interferometers are intentionally unbalanced to allow the extraction of the group index from the measured free spectral range (FSR).**

***Index Terms*—Integrated photonics, Mach-Zehnder interferometer, group index extraction, free spectral range, slow-light waveguides, sub-wavelength gratings.**

I. Introduction

Silicon photonics has emerged as a key technology for the realization of compact, low-cost, and high-performance optical integrated circuits, enabling applications in optical communications, sensing, and signal processing. Silicon photonics leverages the existing CMOS manufacturing infrastructure, enabling large-scale production [1]. Among integrated photonic devices, interferometric circuits such as the Mach-Zehnder interferometer play a central role in modulation, filtering, and sensing applications. In particular, unbalanced interferometers provide a simple and robust method to extract the waveguide group index by measuring the free spectral range of the transmission spectrum [1], [2]. The objective of this project is the design, simulation, fabrication, and experimental characterization of integrated MZI circuits for the extraction of the waveguide group index. Two different interferometer architectures are investigated: a conventional strip-waveguide MZI and a MZI incorporating a grating waveguide to analyze slow-light effects. The measured results are compared with numerical simulations to validate the models.

II. Theory

A. Waveguide Compact Model

The optical properties of an integrated waveguide can be described using a compact model based on the effective refractive index $n_{\text{eff}}(\lambda)$ and group index. The propagation constant $\beta(\lambda)$ is given by

$$\beta(\lambda) = \frac{2\pi}{\lambda} n_{\text{eff}}(\lambda). \tag{1}$$

The group index is defined as

$$n_g(\lambda) = n_{\text{eff}}(\lambda) - \lambda \frac{dn_{\text{eff}}(\lambda)}{d\lambda}. \tag{2}$$

Course: edX Silicon Photonics Design, Fabrication and Data Analysis.
Affiliation: Politecnico di Torino, Turin, Italy.
edX Public Username: SALVATORESALPIETRO

B. Mach–Zehnder Interferometer Transfer Function

An unbalanced MZI consists of two arms with a path length difference $\Delta L = L_2 - L_1$. Assuming ideal 50/50 splitters, the normalized transmission at the output port can be expressed as

$$T_{\text{MZI}}(\lambda) = \frac{1}{4} \left| e^{-i\beta L_1} + e^{-i\beta L_2} \right|^2 \tag{3}$$

The free spectral range (FSR) of the interferometer is related to the group index by

$$\text{FSR}(\lambda) = \frac{\lambda^2}{n_g(\lambda)\Delta L}. \tag{4}$$

III. Modelling and Simulation

A. Waveguide Geometries and Circuit Designs

Two interferometric modulators are considered, each implemented in two distinct configurations. Both interferometric modulators are designed for quasi-TE polarization using strip waveguides with a fixed silicon thickness of $220\,\text{nm}$, as imposed by the fabrication process and a waveguide width of $500\,\text{nm}$. In the second modulator architecture, one interferometer arm incorporates a grating waveguide. The grating is characterized by a corrugation width of $0.25\,\mu\text{m}$ and a grating period of $0.305\,\mu\text{m}$. These parameters are chosen to induce a slow-light effect and to position the band edge of the dispersion diagram around $1543\,\text{nm}$. Two grating lengths are investigated, corresponding to 850 and 1200 periods, to ensure sufficient accumulated group delay for measuring the wavelength dependence of the group index n_g near the band edge, at the expense of increased spectral ripples due to the higher effective reflectivity of longer gratings. In addition to the interferometric devices, two reference structures consisting of grating waveguides placed between two grating couplers, with the same geometrical parameters as those employed in the two MZI configurations, are included to enable an independent characterization of the two gratings. For circuit interconnections and power splitting, standard components from the EBeam library are employed, including the broadband directional coupler `ebeam_bdc_te1550` and the adiabatic Y-branch splitter `ebeam_y_adiabatic_500pin`.

B. Strip Waveguide Mode Analysis

The fundamental guided mode of the strip waveguide is simulated using *Lumerical MODE Solutions*. The simulated electric field amplitude profile of the fundamental quasi-TE mode is shown in Fig. 1. This mode exhibits an effective index of $n_{\text{eff}} = 2.44$ at a wavelength of $1550\,\text{nm}$, and a corresponding group index of $n_g = 4.20$.

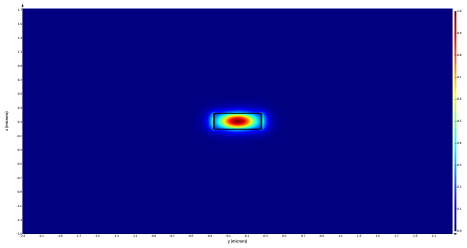

Fig. 1. Simulated fundamental quasi-TE mode profile for a strip waveguide with width $500\,\mathrm{nm}$ and height $220\,\mathrm{nm}$.

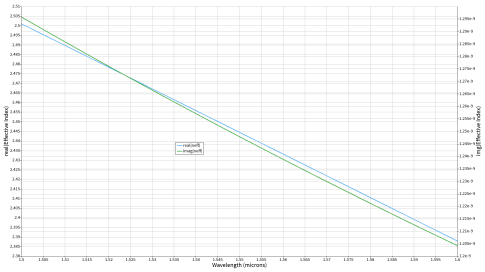

Fig. 2. Simulated effective index n_{eff} as a function of wavelength for the strip waveguide.

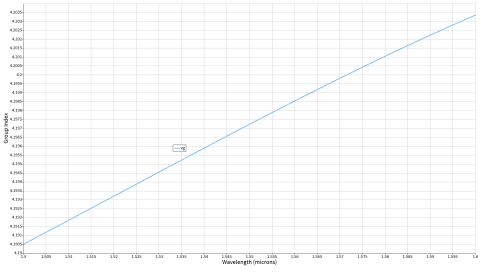

Fig. 3. Simulated group index n_g as a function of wavelength for the strip waveguide.

C. Effective and Group Index Simulations

The effective index n_{eff} and group index n_g of the strip waveguide are computed as a function of wavelength over the range $1500\,\mathrm{nm}$ to $1600\,\mathrm{nm}$. These are obtained directly from the finite difference eigenmode simulations in Lumerical Mode.

Figure 2 reports the simulated effective index as a function of wavelength, while Fig. 3 shows the group index.

D. Waveguide Compact Model (Strip, $width = 500\,\mathrm{nm}$, TE)

A compact model for the strip waveguide is derived from the simulated effective index data exported from *Lumerical MODE Solutions*. The dataset consists of 20 wavelength points uniformly distributed in the $1.50\,\mu\mathrm{m}$ to $1.60\,\mu\mathrm{m}$ range, together with the corresponding complex effective index values $n_{\mathrm{eff}}(\lambda)$.

A second-order Taylor expansion around the center wavelength $\lambda_0 = 1.55\,\mu\mathrm{m}$ is adopted as the waveguide compact model:

$$n_{\mathrm{eff}}(\lambda) = a_0 + a_1(\lambda - \lambda_0) + a_2(\lambda - \lambda_0)^2. \tag{5}$$

The polynomial coefficients are estimated using a fitting procedure implemented in MATLAB. For the strip waveguide with width $500\,\mathrm{nm}$ and quasi-TE polarization, the fitted parameters are:

$$[a_0,\ a_1,\ a_2] = [2.44,\ -1.13,\ -0.04]\,. \tag{6}$$

The fitted model shows excellent agreement with the simulated data over the entire wavelength range, confirming the validity of the second-order approximation. From the compact model, the group index is obtained as

$$n_g(\lambda) = n_{\mathrm{eff}}(\lambda) - \lambda \frac{dn_{\mathrm{eff}}}{d\lambda}, \tag{7}$$

where

$$\frac{dn_{\mathrm{eff}}}{d\lambda} = a_1 + 2a_2(\lambda - \lambda_0). \tag{8}$$

E. Adiabatic Y-branch Design and Characterization

The optical power splitting in the interferometric circuits is implemented using an adiabatic Y-branch in order to ensure low reflection, broadband operation, and equal power splitting over the wavelength range of interest. The Y-branch is first analyzed using a variational FDTD approach to obtain a preliminary estimate of the transmission spectrum and to verify correct power splitting behavior. Subsequently, a full 3D FDTD simulation is performed to extract the scattering parameters (S-parameters) of the device. A mode source exciting the fundamental quasi-TE mode is placed at the input waveguide (Port 1). Three frequency-domain monitors are positioned at the input and output ports to record the transmitted and reflected power. The wavelength sweep spans the range $1.50\,\mu\mathrm{m}$ to $1.60\,\mu\mathrm{m}$. The simulated transmission spectra at the three ports are shown in Fig. 4, Fig. 5 and Fig. 6. When light is injected from Port 1, the optical power is evenly split between the two output ports, with each arm carrying approximately 50% of the input power across the entire wavelength range.

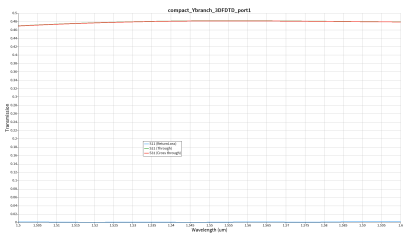

Fig. 4. Simulated transmission and reflection coefficients of the adiabatic Y-branch obtained from 3D FDTD simulations when the fundamental TE mode is injected into Port 1.

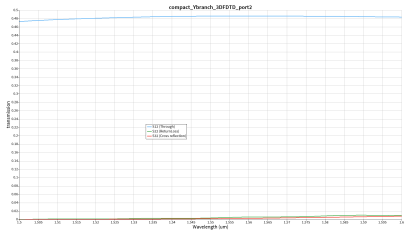

Fig. 5. Simulated transmission and reflection coefficients of the adiabatic Y-branch obtained from 3D FDTD simulations when the fundamental TE mode is injected into Port 2.

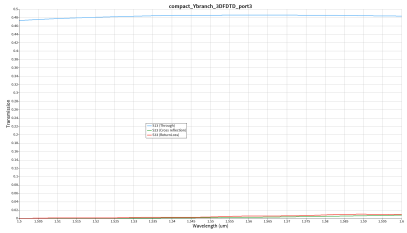

Fig. 6. Simulated transmission and reflection coefficients of the adiabatic Y-branch obtained from 3D FDTD simulations when the fundamental TE mode is injected into Port 3.

F. Mach–Zehnder Interferometer Transfer Function

The optical transfer function of an unbalanced Mach-Zehnder interferometer (MZI) can be expressed as a function of the optical wavelength by considering the phase difference accumulated between the two interferometer arms. Assuming ideal $50:50$ couplers and equal propagation losses in both arms, the normalized transmission at the output port of an imbalanced interferometer with identical waveguides can be expressed as

$$T(\lambda) = \frac{1}{2}\left[1 + \cos(\Delta\phi(\lambda))\right], \tag{9}$$

where $\Delta\phi(\lambda)$ is the wavelength-dependent phase difference between the two arms.

The phase difference is given by

$$\Delta\phi(\lambda) = \frac{2\pi}{\lambda}\, n_{eff}(\lambda)\, \Delta L, \tag{10}$$

where $n_g(\lambda)$ is the waveguide group index and $\Delta L = L_2 - L_1$ is the path length difference between the two interferometer arms.

The periodicity of the transfer function in wavelength corresponds to the free spectral range (FSR), defined as

$$\mathrm{FSR}(\lambda) = \frac{\lambda^2}{n_g(\lambda)\, \Delta L}. \tag{11}$$

Equations (9)–(11) describe the wavelength-dependent response of the interferometer and form the basis for extracting the waveguide group index from the measured transmission spectrum.

G. Parameter variations and expected performance (FSR check)

Two identical unbalanced MZI modulators were implemented using quasi-TE strip waveguides ($220\,\mathrm{nm}$ Si thickness, $500\,\mathrm{nm}$ width). The two layouts differ only in the path-length imbalance $\Delta L = L_2 - L_1$.
Using the simulated free spectral range (FSR) at $1550\,\mathrm{nm}$ and applying equation (11), the group index was extracted, yielding $n_g = 4.22$ for $\Delta L = 210.10\,\mu\mathrm{m}$ and $n_g = 4.12$ for $\Delta L = 397.10\,\mu\mathrm{m}$.

TABLE I
DESIGN VARIATIONS AND EXPECTED PERFORMANCE FOR THE TWO MZI MODULATORS.

Modulator	*width* (nm)	ΔL (µm)	FSR@1550 nm (nm)	n_g
MZI_1 (smaller ΔL)	500	210.10	2.71	4.22
MZI_2 (larger ΔL)	500	397.10	1.47	4.12

The selected path length differences ΔL result in free spectral ranges of $2.71\,\mathrm{nm}$ for MZI_1 ($\Delta L = 210.10\,\mu\mathrm{m}$) and $1.47\,\mathrm{nm}$ for MZI_2 ($\Delta L = 397.10\,\mu\mathrm{m}$) at $\lambda = 1550\,\mathrm{nm}$. Over the wavelength range $1500\,\mathrm{nm}$ to $1600\,\mathrm{nm}$, the FSR remains almost constant (Fig. 7). These FSR values are compatible with laboratory measurements, which provide a spectral bandwidth of about $50\,\mathrm{nm}$ around $1550\,\mathrm{nm}$ and a minimum wavelength resolution on the order of $1\,\mathrm{pm}$.

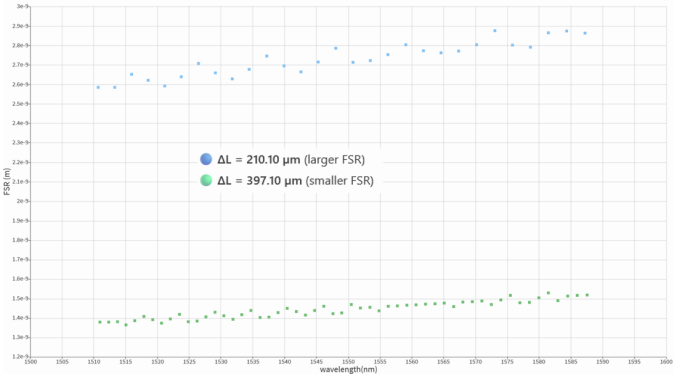

Fig. 7. Simulated free spectral range (FSR) as a function of wavelength for the two MZI modulators with different path-length imbalance ΔL.

From experimental data, the group index will be extracted following the same procedure used for the simulated data. A swept-wavelength measurement of the MZI transmission spectrum will be performed using a tunable laser source and an optical spectrum analyzer. The free spectral range will be obtained by measuring the wavelength spacing between consecutive transmission maxima (or minima). Finally, the waveguide group index will be calculated using the equation (11) evaluated at the central wavelength of interest.

H. Transmission Spectrum of the Mach–Zehnder Interferometers

Figure 8 shows the simulated transmission spectra of the two Mach–Zehnder interferometers, obtained from circuit-level simulations. The spectra are reported as optical gain

versus wavelength for the two devices, which differ only in the path length difference ΔL between the interferometer arms.

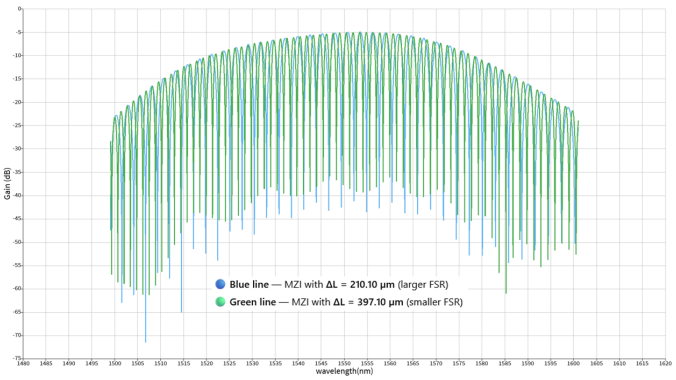

Fig. 8. Simulated transmission spectra of the two Mach–Zehnder interferometers with different path length differences ΔL.

In both cases, the transmission spectrum is modulated by a smooth envelope centered around $1550\,\mathrm{nm}$, mainly determined by the grating couplers and waveguide losses.

I. Effect of Slow-Light Grating

An analogous analysis is carried out for the additional two Mach–Zehnder interferometers (MZI_3 and MZI_4), which differ from MZI_1 and MZI_2 by the presence of a slow-light grating waveguide in one interferometer arm. The grating geometry (corrugation width and period) is kept identical to the one described previously and the grating periods are 1200 and 850, respectively. For each device, the length of the reference arm (without grating) is adjusted such that it matches the length of the grating arm excluding the grating section. Figure 9 shows the simulated transmission spectra of MZI_3 and MZI_4. Compared to the uniform-waveguide interferometers, as the wavelength approaches the grating band edge, the transmission becomes increasingly distorted and irregular.

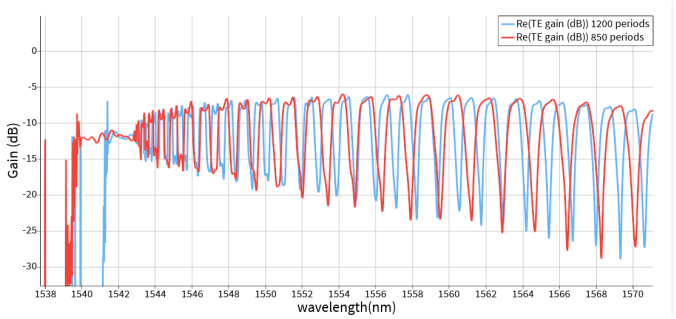

Fig. 9. Simulated transmission spectra of MZI_3 and MZI_4, including a slow-light grating waveguide with 1200 and 850 periods, respectively.

The corresponding free spectral range extracted from the transmission spectra is reported in Fig. 10. In contrast to the nearly constant FSR observed for MZI_1 and MZI_2, the FSR of MZI_3 and MZI_4 decreases significantly as the wavelength approaches the band edge. This behavior is a direct consequence of the strong increase of the group index near the grating band edge in the slow-light regime.

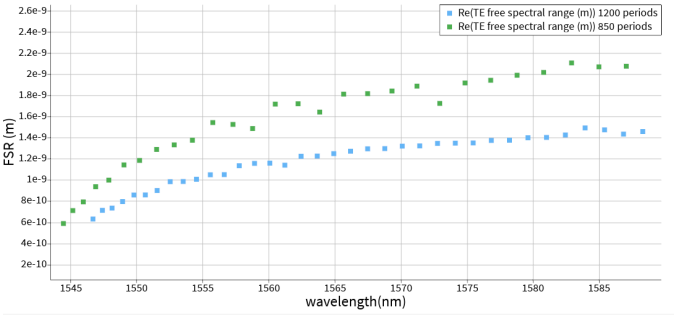

Fig. 10. Free spectral range as a function of wavelength for MZI_3 and MZI_4. The FSR decreases as the wavelength approaches the grating band edge due to the increasing group index.

Close to the band edge, the transmission spectra become irregular. This effect arises from a strong backscattering. To mitigate this effect the introduction of adiabatic tapers between the strip waveguide and the slow-light grating section would be required in a practical implementation.

IV. Fabrication

The photonic devices designed in this work were fabricated within the framework of the edX UBCx Phot1x Silicon Photonics Design, Fabrication and Data Analysis course. Figure 11 shows the layout of the fabricated chip.

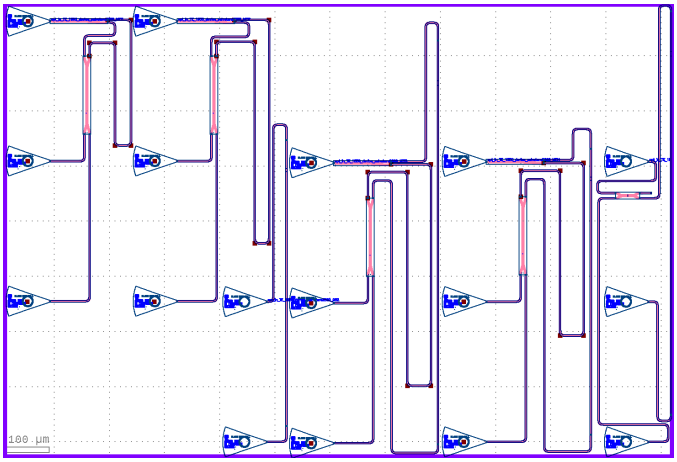

Fig. 11. Chip layout used for fabrication.

V. Experimental Data

VI. Analysis

VII. Conclusion

VIII. Acknowledgements

I acknowledge the edX UBCx Phot1x Silicon Photonics Design, Fabrication and Data Analysis course, which is supported by the Natural Sciences and Engineering Research Council of Canada (NSERC) Silicon Electronic-Photonic Integrated Circuits (SiEPIC) Program. The devices were fabricated by Richard Bojko at the University of Washington Washington Nanofabrication Facility, part of the National Science Foundation's National Nanotechnology Infrastructure Network (NNIN), and Cameron Horvath at Applied Nanotools, Inc.

Enxiao Luan performed the measurements at The University of British Columbia. I acknowledge Lumerical Solutions, Inc., Mathworks, Mentor Graphics, Python, and KLayout for the design software.

REFERENCES

[1] Lukas Chrostowski, Michael Hochberg. Silicon Photonics Design. Cambridge University Press (CUP), 2015.

[2] Lukas Chrostowski, Michael Hochberg. Testing and packaging. 381–405 In Silicon Photonics Design. Cambridge University Press (CUP).

[3] Yun Wang, Xu Wang, Jonas Flueckiger, Han Yun, Wei Shi, Richard Bojko, Nicolas A. F. Jaeger, Lukas Chrostowski. Focusing sub-wavelength grating couplers with low back reflections for rapid prototyping of silicon photonic circuits. Opt. Express 22, 20652 The Optical Society, 2014.